International Symposium
On Turbulence and Shear Flow
Phenomena (TSFP-8)
August 28 - 30, 2013 Poitiers, France

EFFECTS OF RADIATIVE HEAT TRANSFER ON THE TURBULENCE STRUCTURE IN REACTING AND INERT MIXING LAYERS

Somnath Ghosh, Rainer Friedrich and Christian Stemmer
Lehrstuhl für Aerodynamik und Strömungsmechanik, Technical University of Munich
Boltzmannstr. 15, D-85748 Garching, Germany
Somnath.Ghosh@aer.mw.tum.de, R.Friedrich@lrz.tum.de

Benedicte Cuenot[1] and Mouna El Hafi[2]
[1]CERFACS-CFC/Combustion, 42 Avenue G. Coriolis, 31057 Toulouse, France
[2]Laboratoire de Génie des Procédés des Solides Divisés, Ecole des Mines d'Albi, 81013 Albi, France

ABSTRACT

We use large-eddy simulation to study the interaction between turbulence and radiative heat transfer in low-speed inert and reacting plane temporal mixing layers. An explicit filtering scheme based on approximate deconvolution is applied to treat the closure problem arising from quadratic nonlinearities of the filtered transport equations. In the reacting case, the working fluid is a mixture of ideal gases where the low-speed stream consists of hydrogen and nitrogen and the high-speed stream of oxygen and nitrogen. Both streams are premixed in a way that the free-stream densities are the same and the stoichiometric mixture fraction is 0.3. The filtered heat release term is modelled using equilibrium chemistry. In the inert case the low-speed stream consists of nitrogen at a temperature of 1000 K and the high-speed stream is pure water vapour of 2000 K, when the radiation is turned off. Simulations assuming the gas mixtures as grey gases with artificially increased Planck mean absorption coefficients are performed in which the LES code and the radiation code PRISSMA are fully coupled. In both cases radiative heat transfer is found to clearly affect fluctuations of thermodynamic variables, Reynolds stresses and budget terms like pressure-strain correlations. Source terms in the transport equation for the variance of temperature fluctuations are used to explain the decrease of this variance in the reacting case and its increase in the inert case.

INTRODUCTION

Thermal radiation is a phenomenon of much longer range in general than heat conduction and convection. Hence partial differential equations describe heat transport by conduction and convection while an integro-differential equation is needed to predict the directional dependence of the radiative intensity in absorbing and emitting gases. A further complication arises from the fact that radiative properties of gases generally vary strongly with the wavenumber of radiation. Due to these difficulties which imply enormous costs of numerical simulations, effects of radiative heat transfer are frequently neglected even in situations where they play a role. While most work on turbulence-radiation-interaction (TRI) has been devoted to the influence of turbulence on radiation, much less work has concentrated on the question of how radiation affects turbulence variables. It is the aim of this contribution to focus on the behaviour of the turbulence structure under the influence of thermal radiation. Concerning the prediction techniques for TRI, a very good compromise with respect to accuracy and cost is achieved by performing a large-eddy simulation (LES) of the flow field, applying the discrete ordinate method (DOM, Modest, 2003) to solve the radiative transfer equation (RTE) for an absorbing-emitting gas and to use the Statistical Narrow Band correlated-K (SNB-cK) model to account for the radiative properties of the gas. The present authors (Ghosh et al., 2011) followed this approach to investigate effects of radiation in supersonic turbulent channel flow with pure water vapour as working gas and friction Reynolds numbers, based on channel half-width of 1026 and above. The computations led to low optical thicknesses and hence weak effects of radiation on the turbulence structure. A natural way to increase the optical thickness of the shear layer would have been to increase the channel half-width by an order of magnitude or more. This would have led to intractable computational costs. Therefore, we have adopted a procedure proposed by Gupta et al. (2009), assuming a grey gas model with a Planck mean absorption coefficient which is artificially increased and varies as a fifth-order polynomial of the inverse temperature. The same procedure is applied here.

When performing LES, the question arises whether subgrid-scale effects play a role in the filtered RTE. In a recent paper Roger et al. (2010) investigate incompressible homogeneous isotropic turbulence, using DNS, with fluctuations of temperature and species concentrations defined through fluctuations of a passive scalar. They find with respect to the RTE integrated over the spectrum, that the strongest subgrid-scale correlations are the temperature self-correlation and the absorption coefficient-temperature correlation. Since these two have opposite effects, the authors conclude that it is better to neglect both correlations in an LES, instead of modelling only one, namely the SGS radiative emission (Roger et al., 2009). Subgrid-scale effects

on radiative emission and absorption have also been neglected by Jones and Paul (2005) and Amaya et al. (2010). Jones and Paul perform an LES of combustion in a gas turbine combined with a solution of the filtered RTE using DOM. An absorbing-emitting, non-scattering grey medium, consisting of water vapour and carbon dioxide is assumed. The challenges of this work are fully-coupled efficient solutions of radiative heat transfer and LES of flow, temperature and composition in a general body-fitted coordinate system. In an ambitious piece of work Amaya et al. (2010) couple three different solvers directly, namely an LES solver for flow and chemistry, the radiation solver PRISSMA and a solver for heat conduction into solids in order to evaluate the impact of heat conduction into a blade and radiation on the thermal behaviour of the blade in the distributor downstream of a helicopter combustion chamber. The radiation solver uses DOM with different angular discretizations. Radiative gas properties are taken care of with a tabulated FS-SNBcK spectral model, focusing on emission and absorption and neglecting subgrid-scale effects. The results show that both, heat conduction and radiation have a remarkable impact on the fluid and blade temperatures. Based on the discussion of the cited references and our aim to investigate fundamental effects of radiative heat transfer on the structure of turbulent mixing layers, it seems justified here as well to neglect subgrid-scale effects on radiative emission and absorption in inert and reacting mixing layers.

BASIC EQUATIONS AND NUMERICAL INTEGRATION

The compressible flow equations for a multicomponent thermally radiating mixture of ideal gases read in Cartesian coordinates:

$$\frac{\partial \rho}{\partial t}+\frac{\partial \rho u_j}{\partial x_j}=0, \qquad (1)$$

$$\frac{\partial \rho u_i}{\partial t}+\frac{\partial}{\partial x_j}\left(\rho u_i u_j\right)=-\frac{\partial p}{\partial x_i}+\frac{\partial \tau_{ij}}{\partial x_j}, \qquad (2)$$

$$\rho c_p \frac{DT}{Dt}=-\sum_{\alpha=1}^{N} h_\alpha \omega_\alpha+\frac{Dp}{Dt}+\tau_{ij}s_{ij}$$
$$+\frac{\partial}{\partial x_j}\left(\lambda\frac{\partial T}{\partial x_j}\right)-\frac{\partial q_{j,R}}{\partial x_j}+\frac{\partial T}{\partial x_j}\sum_{\alpha=1}^{N}\frac{c_{p_\alpha}\mu}{Sc}\frac{\partial Y_\alpha}{\partial x_j} \qquad (3)$$

In this set of mass (1), momentum (2) and energy equations (3), ρ, u_i, p, T, h_α, ω_α, Y_α, $q_{i,R}$, s_{ij}, τ_{ij}, μ, λ, c_p, Sc denote density, velocity vector, pressure, temperature, species enthalpy, reaction rate and mass fraction, radiative heat flux vector, deformation tensor, viscous stress tensor, dynamic viscosity, thermal conductivity, specific heat at constant pressure, Schmidt number. Variables without index 'α' are mixture variables. While the molecular transport coefficients are computed efficiently using the code EGLib (Ern & Giovangigli 1995), polynomial expressions are applied to specify the temperature dependence of the specific heats (Gardiner 1984). The case of reacting flow is modelled, using an infinitely fast global reaction and simplified diffusion mechanisms with constant Schmidt number. Species mass fractions are related to a mixture fraction ξ via the Burke-Schumann relations. ξ satisfies the following transport equation:

$$\frac{\partial \rho\xi}{\partial t}+\frac{\partial}{\partial x_j}\left(\rho u_j \xi\right)=\frac{\partial}{\partial x_j}\left(\frac{\mu}{Sc}\frac{\partial \xi}{\partial x_j}\right) \qquad (4)$$

The radiative source term, $\partial q_{j,R}/\partial x_j$ in the energy equation is obtained by integrating the radiative transfer equation (RTE) for a grey, emitting-absorbing gas (Modest, 2003)

$$dI/ds=\kappa I_b-\kappa I \qquad (5)$$

The radiative intensity I depends on the direction s in which the energy propagates and on the location in space, $\vec{x}$. κ, I_b denote the frequency-integrated absorption coefficient and black body radiative intensity. The first term on the right-hand-side of Eq. (5) describes the gain of radiative intensity by emission and the second the loss by absorption. The radiative source term appearing in the energy equation is obtained from (5) through integration over the solid angle Ω:

$$\frac{\partial q_{j,R}}{\partial x_j}=4\pi\kappa I_b-\kappa\int_{4\pi} I d\Omega=\underbrace{4\kappa_P\sigma T^4}_{emission}-\underbrace{\kappa\int_{4\pi} I d\Omega}_{absorption} \qquad (6)$$

κ_P denotes Planck's mean absorption coefficient. σ is the Stefan-Boltzmann constant. The refractive index is assumed constant, equal to one. Following Gupta et al. (2009) we adopt the following form for κ_P:

$$\kappa_P=C_\kappa\left[c_0+c_1\left(\frac{A}{T}\right)+c_2\left(\frac{A}{T}\right)^2+c_3\left(\frac{A}{T}\right)^3+c_4\left(\frac{A}{T}\right)^4+c_5\left(\frac{A}{T}\right)^5\right] \qquad (7)$$

The coefficients c_0 - c_5 and A were taken from a radiation model suggested for water vapor (Sandia National Laboratories, 2002). The coefficient C_κ allows for variation of κ_P independently of the other parameters.

The convection and molecular transport terms of the transport equations (1-4) are discretized, using the compact sixth-order scheme of Lele (1992). A third-order 'low-storage' Runge-Kutta scheme of Williamson (1980) advances the solution in time.

Our LES-approach which has been described and successfully tested against DNS data of inert compressible flow in Mathew et al. (2003, 2006) consists in defining an LES-grid and in filtering the high-order numerical solution explicitly at each time step using the composite filter $(Q_N * G)$. G is a second order Padé filter containing a parameter which allows to control the cutoff wavenumber, and Q_N is the approximate inverse of G, obtained from a van Cittert series which is truncated at N=5. The filtering affects the highest resolved scales only and has the advantage that the LES result tends uniformly to the DNS result as the grid is refined and the filter cut-off is moved towards the highest

wavenumbers. For more details, the reader is referred to the cited literature. When chemical reaction takes place the filtered heat-release term forms an extra closure problem. This is solved here in analogy to a statistical model of Bilger (1980).
The three-dimensional RTE (Eq. (5)) is integrated with the discrete ordinate method implemented in the code PRISSMA. This code uses finite-volume discretizations and a second-order Diamond mean flux scheme (Joseph et al. 2005) to compute I along a line of sight. The flow field and the radiation field are directly coupled such that PRISSMA gets the filtered pressure and temperature fields at about every characteristic convective time interval and the compressible LES solver receives the radiative source term. An explicit filtering of the RTE which produces subgrid-scale contributions involving filtered products of absorption coefficient with radiative intensity and Planck's black body radiative intensity, has been neglected here. PRISSMA has been extensively used and validated e.g. in Amaya et al. (2010).
We would like to point out, that we do not specifically denote LES variables with an overbar or a tilde. From now on, all flow variables are explicitly filtered space- and time-dependent quantities, unless otherwise stated. A variable with an overbar or a tilde represents a statistical average.

FLOW CONFIGURATION

The present temporally evolving mixing layers are parametrized by a Reynolds number (based on vorticity thickness δ_ω), a convective Mach number M_c and an optical thickness τ_H, defined using Planck's mean absorption coefficient $\bar{\kappa}_P$:

$$Re_\omega = \frac{\rho_0 \Delta u \delta_\omega}{\mu_0}, \qquad M_c = \frac{\Delta u}{c_1 + c_2}, \qquad \tau_H = \int_{y=0}^{H} \bar{\kappa}_P(y)dy, \qquad \kappa_P = \frac{\pi \kappa I_b}{\sigma T^4} \tag{8}$$

Δu is the velocity difference between high-speed stream (index 1) and low-speed stream (index 2) and c_1, c_2 are their sonic speeds. ρ_0, μ_0 are averaged free-stream densities and viscosities, e.g. $\rho_0 = (\bar{\rho}_1 + \bar{\rho}_2)/2$. H is the width of the computational domain in y-direction (across the streams). Table 1 lists the initial and final Reynolds numbers and the Mach numbers, together with the optical thicknesses of the mixing layers. Definition (8) of the convective Mach number provides a good approximation for M_c, because the ratio of specific heats of both streams differs by less than 1%.
The computational domain for inert flow of size 129×180×32 in (x, y, z)-directions (stream-, cross- and spanwise) and measured in initial vorticity thicknesses, is discretized by 192×288×48 points. The domain for reacting flow has the size 41.5×21×10.4 in (x, y, z)-directions and is discretized by 192×108×48 points. The mass, momentum and energy (or pressure, temperature and velocity) satisfy periodic boundary conditions in stream- and spanwise directions. In the end planes perpendicular to these directions, fully reflective boundary conditions (with zero emissivity) are imposed in the radiative code PRISSMA. In the cross-stream direction the flow variables satisfy non-reflective boundary conditions. Concerning radiation either the incoming radiative intensity is set to zero or a black-body boundary condition at local temperature is applied.

Table 1: Flow parameters of reacting and inert mixing layers with radiative heat transfer (values in brackets correspond to cases without radiation).

Flow	$Re_{\omega 0}$	$Re_{\omega f}$	M_c	τ_H
reacting	9304	32450	0.15	0.8
	(9304)	(32449)	(0.15)	
inert	533	16082	0.182	0.3
	(533)	(15754)	(0.178)	

RESULTS

Reacting mixing layer

We present statistical results of the reacting temporal mixing layer, taken from self-similar states in which the momentum thickness grows at constant rate. An important first observation is the increase in growth rate when thermal radiation sets in, compared to the non-radiating case. Figure 1 shows the momentum thickness, normalized with its initial value versus non-dimensional time.

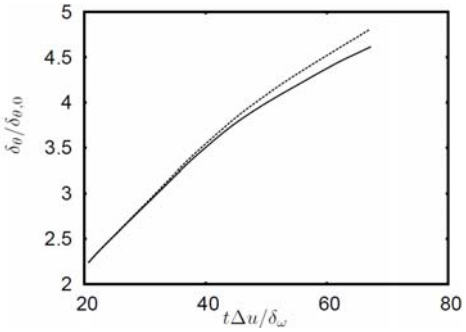

Fig. 1. Momentum thickness versus time. Solid line: no radiation. Dashed line: grey-gas radiation.

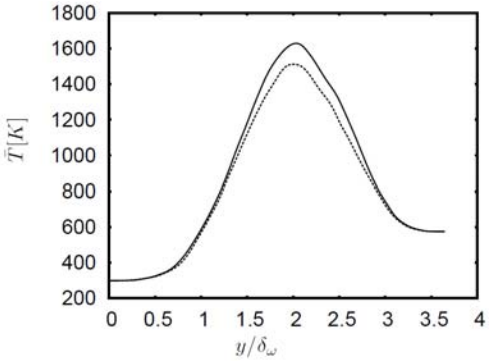

Fig. 2. Mean temperature. Lines as in Fig. 1.

Due to heat of reaction the mean temperature of the mixing layer reaches a maximum value of 1630 K (Fig. 2). Radiation of heat reduces this peak value by 120 K (about 7%). The temperature ratio of the two streams (upward/

downward streams: indices 2,1) is T_2/T_1= 2.03. At initially constant pressure across the layer this guarantees equal densities on both sides. Figure 3 shows the increase in mean density due to thermal radiation. Since there is only a negligible drop of the mean pressure level due to thermal radiation, the increase in mean density reflects the decrease in mean temperature.

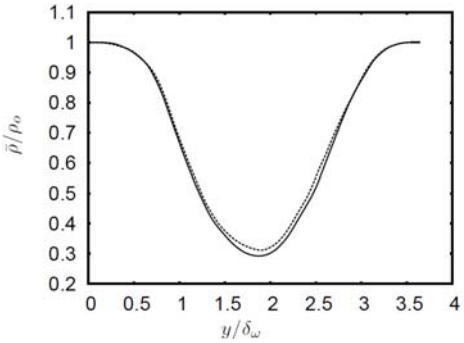

Fig. 3. Mean density. Lines as in Fig. 1.

The mean streamwise velocity remains practically unaffected by thermal radiation (not shown).
The typical double-peak profile of RMS temperature fluctuations reveals relative maxima of 445 and 567 K. These peak values drop by 37 and 83 K, respectively, due to radiation (Figure 4). Corresponding reductions are also noted in density fluctuations (not shown). On the other hand

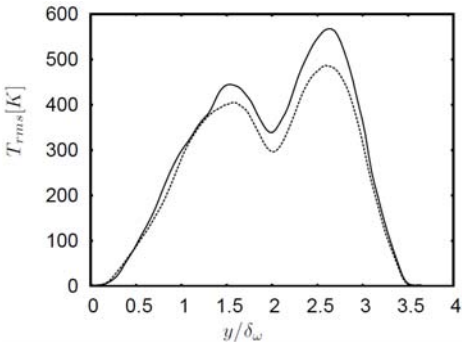

Fig. 4. RMS temperature fluctuations. Lines as in Fig. 1.

pressure fluctuations which are primarily of hydrodynamic nature in this low Mach number case, increase. This points towards an increased activity of the fluctuating velocity field and shows up in the Reynolds stresses. Their peak values increase when radiation is included. We show examples of streamwise and crosswise Reynolds stresses in Figures 5 and 6. This increase in turbulence activity due to thermal radiation - caused by a reduction of mean temperature and an increase of mean density - is also reflected in the production and pressure-strain correlation terms.

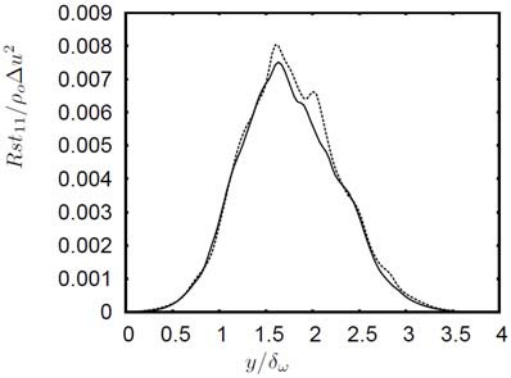

Fig. 5. Streamwise Reynolds stress. Lines as in Fig. 1.

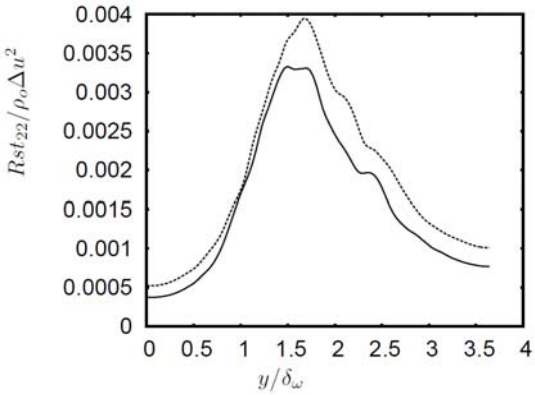

Fig. 6. Crosswise Reynolds stress. Lines as in Fig. 1.

Figures 7 and 8 refer to the corresponding streamwise components only, due to lack of space. The other components show similar behaviours.

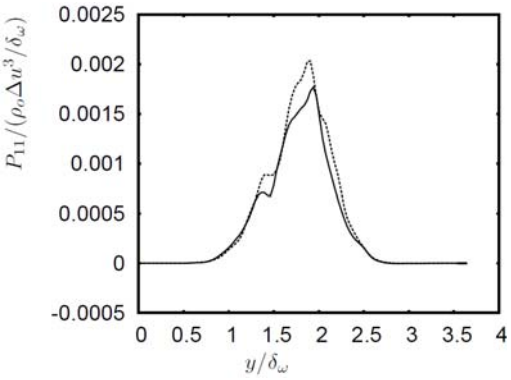

Fig. 7. Production of streamwise Reynolds stress. Lines as in Fig. 1.

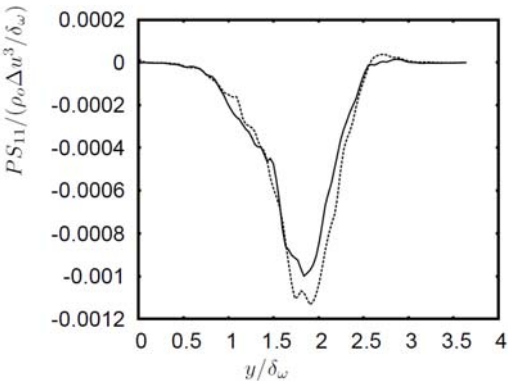

Fig. 8. Pressure-strain correlation in streamwise Reynolds stress balance. Lines as in Fig. 1.

In order to understand the increase in density and temperature fluctuations due to thermal radiation, we study the transport equation for the variance of the temperature fluctuations. It is derived from Eq. (3) and reads:

$$\frac{\partial}{\partial t}\overline{\rho T''^2}+\frac{\partial}{\partial x_j}\left(\widetilde{u}_j\overline{\rho T''^2}\right)=\underbrace{-2\overline{\rho u_j'' T''^2}\frac{\partial \widetilde{T}}{\partial x_j}}_{\text{production}}\underbrace{-2\overline{\frac{T''}{c_p}\sum_{\alpha=1}^{N}h_\alpha\omega_\alpha}}_{\text{heat release}}\underbrace{-2\overline{\frac{T''}{c_p}\frac{\partial q_{j,R}}{\partial x_j}}}_{\text{radiation}}$$
$$\underbrace{-\frac{\partial}{\partial x_j}\overline{\rho u_j'' T''^2}}_{\text{turb.diffusion}}\underbrace{+2\overline{\frac{T''}{c_p}\frac{\partial T}{\partial x_j}\sum_{\alpha}\frac{\mu c_{p\alpha}}{Sc}\frac{\partial Y_\alpha}{\partial x_j}}}_{\text{species diffusion}}\underbrace{+2\overline{\frac{T''}{c_p}\left(\frac{Dp}{Dt}+\tau_{ij}s_{ij}+\frac{\partial}{\partial x_j}\left(\lambda\frac{\partial T}{\partial x_j}\right)\right)}}_{\text{pressure, dissipation, heat conduction}} \quad (9)$$

As known from inert non-radiating flow, the RHS of this equation contains production due to mean temperature gradient, turbulent diffusion and correlation between temperature fluctuation and the sum of pressure gradient, dissipation rate and divergence of conductive heat flux. When heat release, thermal radiation and energy transport by species diffusion play a role in the energy balance, extra correlations between temperature fluctuations and these mechanisms appear and control the behaviour of the temperature variance.

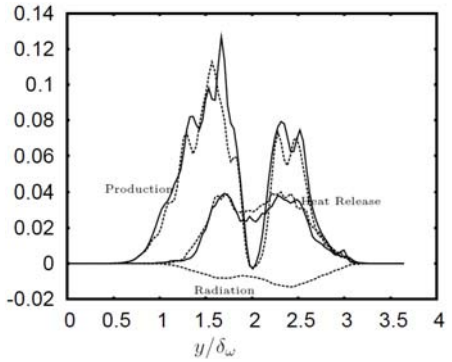

Fig. 9. Source terms in the balance equation (9) for the temperature variance. Lines as in Fig. 1.

In Fig. 9 we show profiles of three major source terms across the mixing layer, normalized with $\rho_0 \Delta u T_0^3/\delta_\omega$. While the production term decreases under the effect of thermal radiation, the heat release term slightly increases. The important contribution to the reduced level of the temperature variance, however, is due to the interaction between temperature fluctuation and radiative source term.

Inert mixing layer

We focus on a few aspects only due to lack of space. Figure 10 shows the increased growth of the normalized momentum thickness, when radiation sets in.

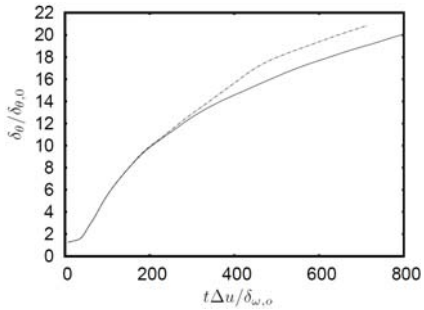

Fig. 10. Momentum thickness versus time. Solid line: no radiation. Dash-dotted line: grey-gas radiation.

The mean temperature of the mixing layer's hot side decreases by roughly 5% due to thermal radiation (Fig. 11). At the same time all mean flow profiles are shifted towards the low-density side. An analogous shift of profiles was also observed in DNS of temporal mixing layers by Pantano & Sarkar (2002) when the density ratio was increased.

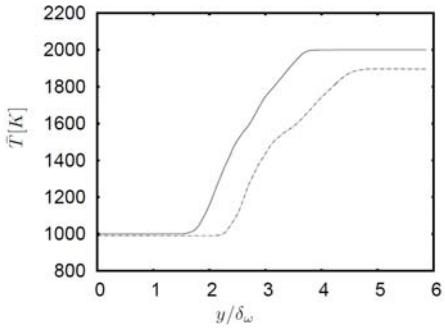

Fig. 11. Mean temperature. Solid line: no radiation. Dashed line: grey-gas radiation.

A similar increase in the turbulence activity as in the reacting mixing layer leads to an enhancement of all the Reynolds stresses. As an example we show the stress in the y-direction in Fig. 12.

It comes as a surprise, however, that the temperature and density fluctuations increase when radiation is included. Fig. 13 presents the temperature fluctuations. The explanation for this contrasting behaviour is provided by the dominant source terms in Eq. (9).

While the production of temperature fluctuations strongly increases, the interaction between temperature fluctuations and the radiative source term is very small (Fig. 14). Terms related to reaction and species diffusion do not appear.

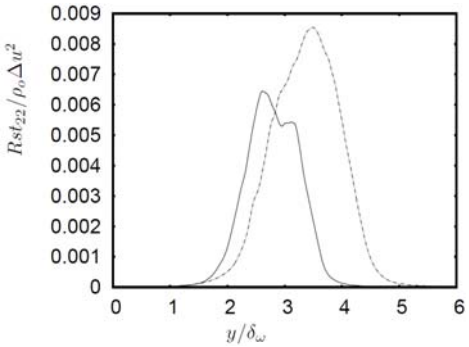

Fig. 12. Crosswise Reynolds stress. Lines as in Fig. 10.

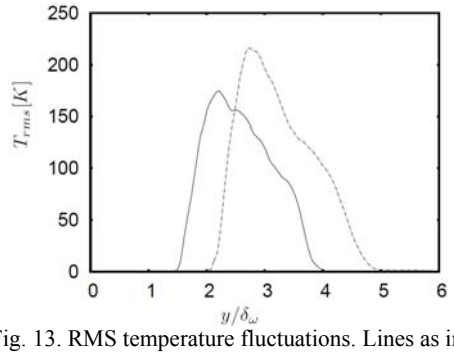

Fig. 13. RMS temperature fluctuations. Lines as in Fig. 10.

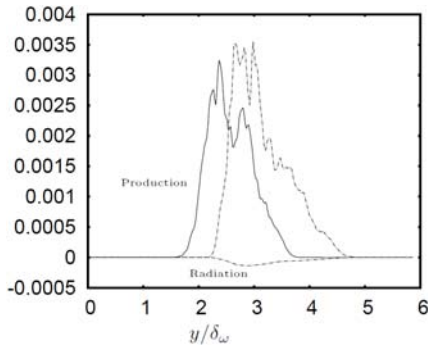

Fig. 14. Source terms in the balance equation (9) for the temperature variance. Lines as in Fig. 10.

Acknowledgement

The first author (S.G.) acknowledges the financial support received from Deutsche Forschungsgemeinschaft within the research project FR 478/25-1.

REFERENCES

Amaya, J., Collado, E., Cuenot, B. and Poinsot, T., 2010, "Coupling LES, radiation and structure in gas turbine simulations." *CTR, Proc. Summer Program*, pp. 239-249.

Bilger, R.W., 1980, "Turbulent flows with nonpre-mixed reactants." – In: *Topics in Applied Physics*, Eds. P.A. Libby and F.A. Williams, Springer Verlag, Vol. 44, pp. 65-114.

Ern, A., Giovangigli, V., 1995, "Fast and accurate multicomponent transport property evaluation." *J. Comp. Phys.* 120, pp. 105-116.

Gardiner, W., 1984, *Combustion chemistry*. Springer, New York.

Ghosh, S., Friedrich, R., Pfitzner, M., Stemmer, Chr., Cuenot, B., and El Hafi, M., 2011, "Effects of radiative heat transfer on the structure of turbulent supersonic channel flow." *J. Fluid Mechanics* 677, pp. 417-444 doi:10.1017/jfm.2011.92.

Gupta, A., Modest, M.F., and Haworth, D.C., 2009, "Large eddy simulation of turbulence-radiation interactions in a turbulent planar channel flow." *J. Heat Transfer* 131, pp. 061704.

Joseph, D., Hafi, M.El., Fournier, R. & Cuenot, B., 2005, "Comparison of three spatial differencing schemes in discrete ordinates method using three-dimensional unstructured grids". *Intl J. Therm. Sci.* 44, pp. 851-864.

Jones, W.P., and Paul, M.C., 2005, "Combination of DOM with LES in a gas turbine combustor." *Int. J. Engineering Science* 43, pp. 379-397.

Lele, S.K., 1992, "Compact finite difference schemes with spectral-like resolution." *J. Comp. Phys.* 103, pp. 16-42.

Mathew, J., Lechner, R., Foysi, H., Sesterhenn, J., Friedrich, R., 2003, "An explicit filtering method for large-eddy simulation of compressible flows." *Phys. Fluids* 15, pp. 2279-2289.

Mathew, J., Foysi, H. & Friedrich, R., 2006, "A new approach to LES based on explicit filtering." *Intl J. Heat and Fluid Flow,* 27, pp. 594-602.

Modest, M.F., 2003, *Radiative Heat Transfer*. 2nd Edition. Academic Press.

Pantano, C., and Sarkar, S., 2002, "A study of compressibility effects in the high-speed turbulent shear layer using direct simulation." *J. Fluid Mechanics* 451, pp. 329-371.

Roger, M., Coelho, P.J., da Silva, C.B., 2009, "Analysis of the turbulence-radiation interactions for large eddy simulations of turbulent flows." *Int. J. Heat Mass Transfer* 52, pp. 2243-2254.

Roger, M., Coelho, P.J., da Silva, C.B., 2010, "The influence of the non-resolved scales of thermal radiation in large eddy simulation of turbulent flows: A fundamental study." *Int. J. Heat Mass Transfer* 53, pp. 2897-2907.

Williamson, J.K., 1980, "Low-storage Runge-Kutta schemes." *J. Comp. Phys.* 35, pp. 48-56.